CHEMISTRY
A EUROPEAN JOURNAL

Supporting Information

An Isoreticular Family of Microporous Metal–Organic Frameworks Based on Zinc and 2-Substituted Imidazolate-4-amide-5-imidate: Syntheses, Structures and Properties

Franziska Debatin,[a] Karsten Behrens,[a] Jens Weber,[b] Igor A. Baburin,[c] Arne Thomas,[d] Johannes Schmidt,[d] Irena Senkovska,[e] Stefan Kaskel,[e] Alexandra Kelling,[a] Niklas Hedin,[f] Zoltan Bacsik,[f] Stefano Leoni,[c] Gotthard Seifert,[c] Christian Jäger,[g] Christina Günter,[h] Uwe Schilde,[a] Alwin Friedrich,[a] and Hans-Jürgen Holdt*[a]

chem_201200889_sm_miscellaneous_information.pdf

Experimental Details

Synthesis of IFP-2, IFP-3 and IFP-4 were performed in seal tubes from Ace Glass. All reagents and solvents were used as purchased from great chemical suppliers without further purification if not stated otherwise.

The linker precursors 2-chloro-4,5-dicyanoimidazole[1] (1b), 2-bromo-4,5-dicyanoimidazole[2] (1c) and 2-ethyl-4,5-dicyanoimidazole[3] (1d) were synthesized following published procedures.

Elemental analysis and ICP-OES

Elemental analysis (C, H, N) was performed on Elementar Vario EL elemental analyzer.
ICP-OES was performed on the Perkin Elmer Optical Emission Spectrometer Optima 5300 DV (Scott-Chamber/Cross-Flow-Nebulizer). Zn was observed at $\lambda = 213.8$ nm.

IR spectra

IR spectra were recorded on FT-IR Nexus from Thermo Nicolet in the region of 4000 – 400 cm^{-1} using KBr pellets as basis.

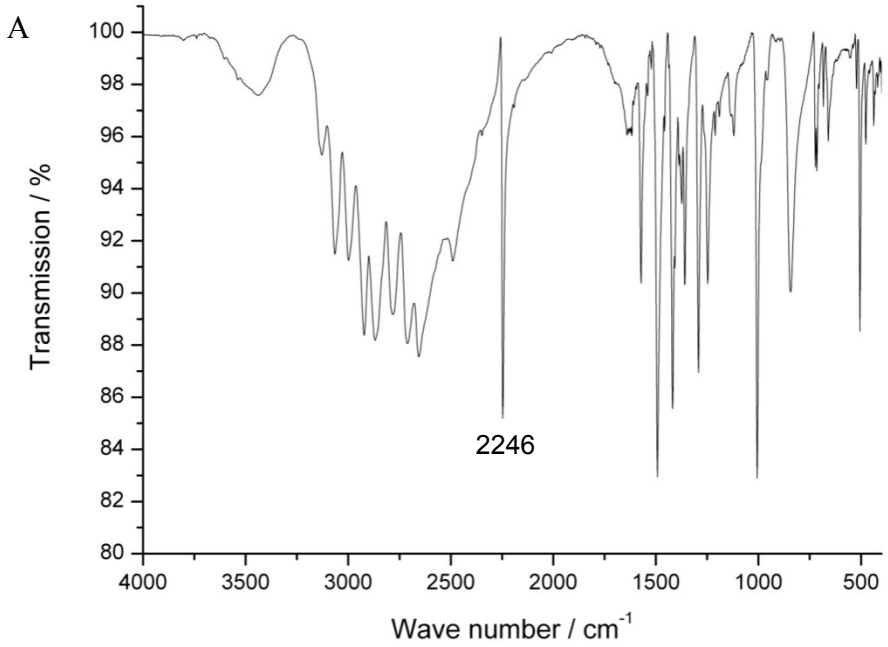

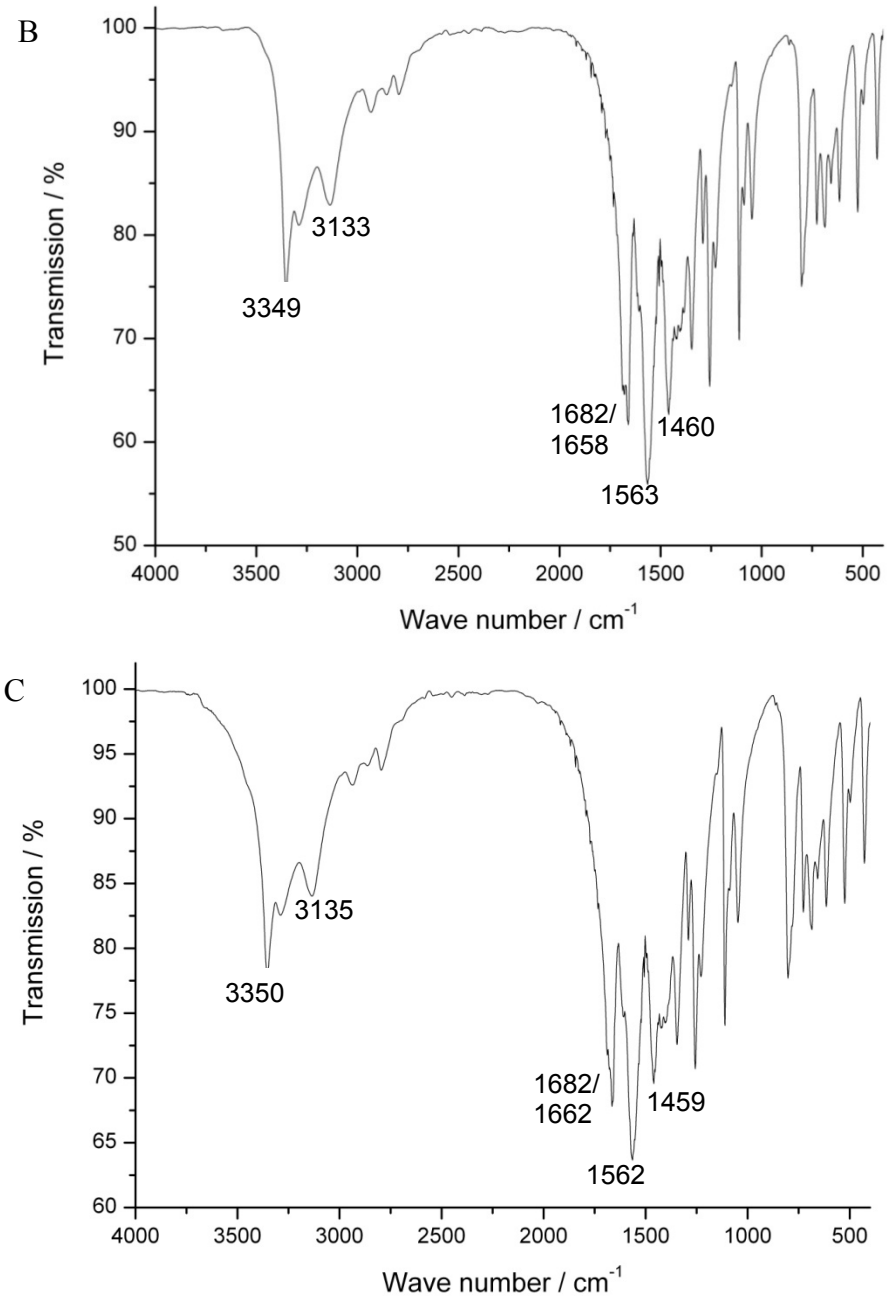

Figure S1-1 IR-spectra of: **A**) 2-chloro-4,5-dicyanoimidazole (1b); **B**) IFP-2 as synthesized; **C**) IFP-2 activated at 200°C and 10^{-3} mbar for 3 days.

A

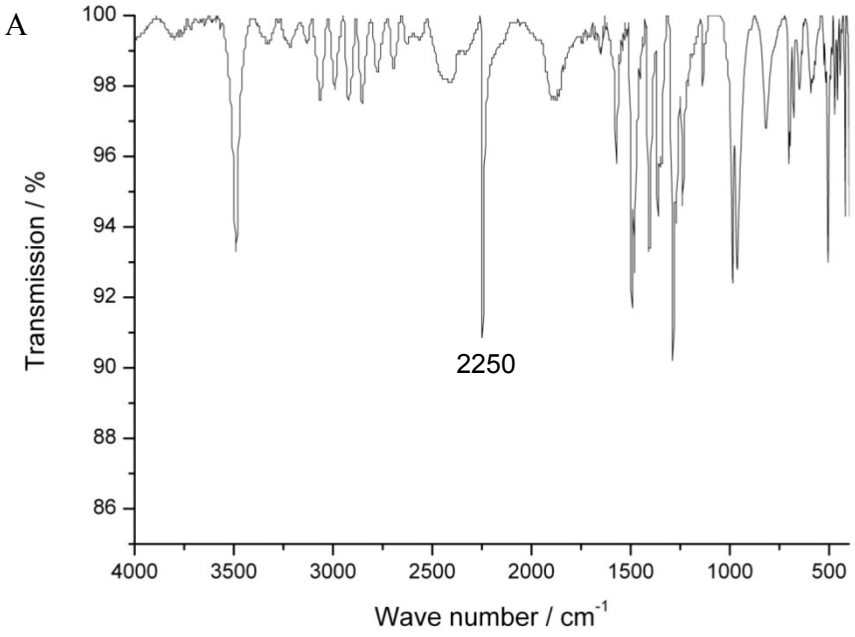
Transmission / %
100
98
96
94
92
90
88
86
2250
4000
3500
3000
2500
2000
1500
1000
500
Wave number / cm-1

B

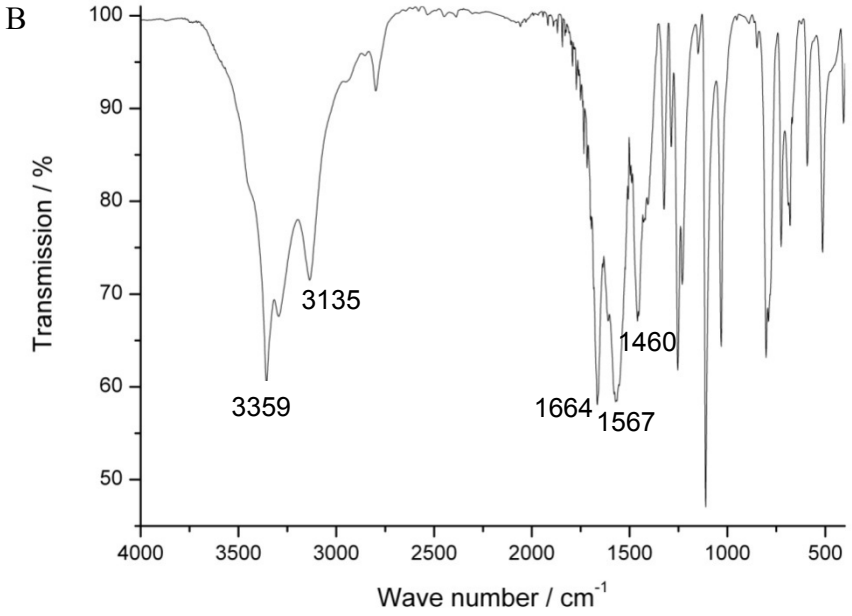
Transmission / %
100
90
80
70
60
50
3359
3135
1664
1567
1460
4000
3500
3000
2500
2000
1500
1000
500
Wave number / cm-1

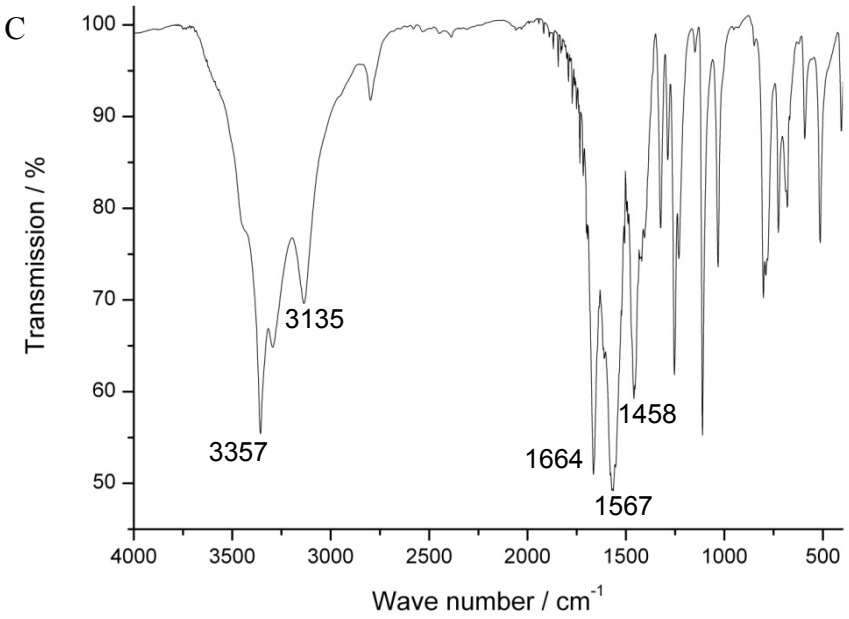

Figure S1-2 IR-spectra of: **A**) 2-bromo-4,5-dicyanoimidazole (1c); **B**) IFP-3 as synthesized; **C**) IFP-3 activated at 200°C and 10^{-3} mbar for 3 days.

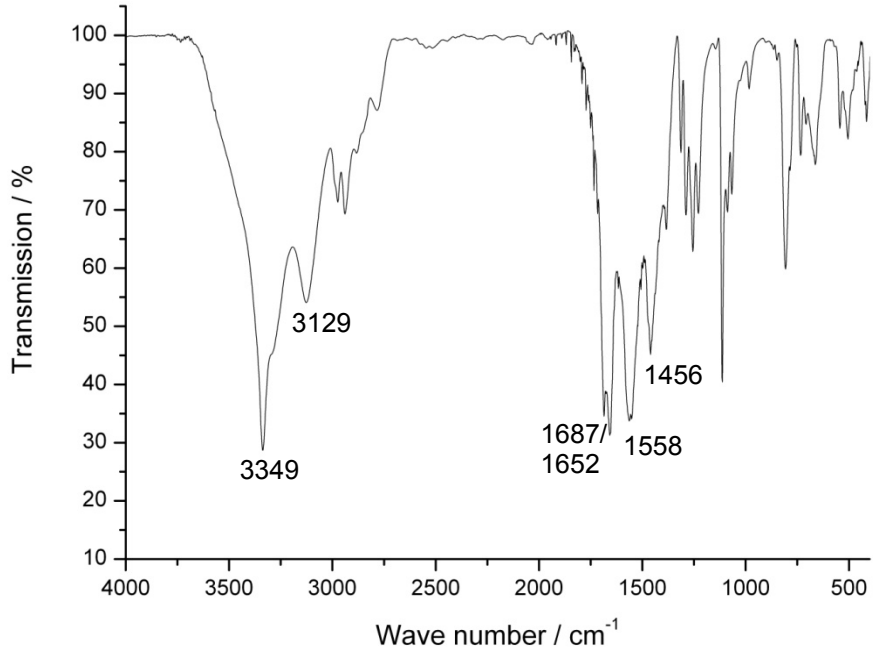

Figure S1-3 IR-spectra of IFP-4 activated at 200°C and 10^{-3} mbar for 3 days.

^{1}H and ^{13}C CPMAS NMR Spectroscopy

^{1}H-^{13}C Cross Polarization experiments with Magic Angle Sample Spinning (^{13}C CPMAS NMR) for IFP-2, IFP-3 and IFP-4 were performed on a Bruker Avance 600 spectrometer (Bruker Biospin GmbH, Rheinstetten, Germany, B_0 = 14.1 T) operating at a frequency of 150.9 MHz using a double resonant 4 mm MAS (magic angle sample spinning) probe. The spinning frequency was 12.5 kHz. For CP, a ramped (50% ramp) lock field was used on the ^{1}H channel with a CP contact time of 2 ms, a recycle delay of 3 s and 512 scans. The 90° ^{1}H pulse length was 3.3 µs. High power TPPM decoupling was applied (B_1 = 80 kHz). The ^{13}C chemical shifts are referenced using the glycine carboxyl group signal ($\delta(^{13}C)$ = 176.4 ppm).

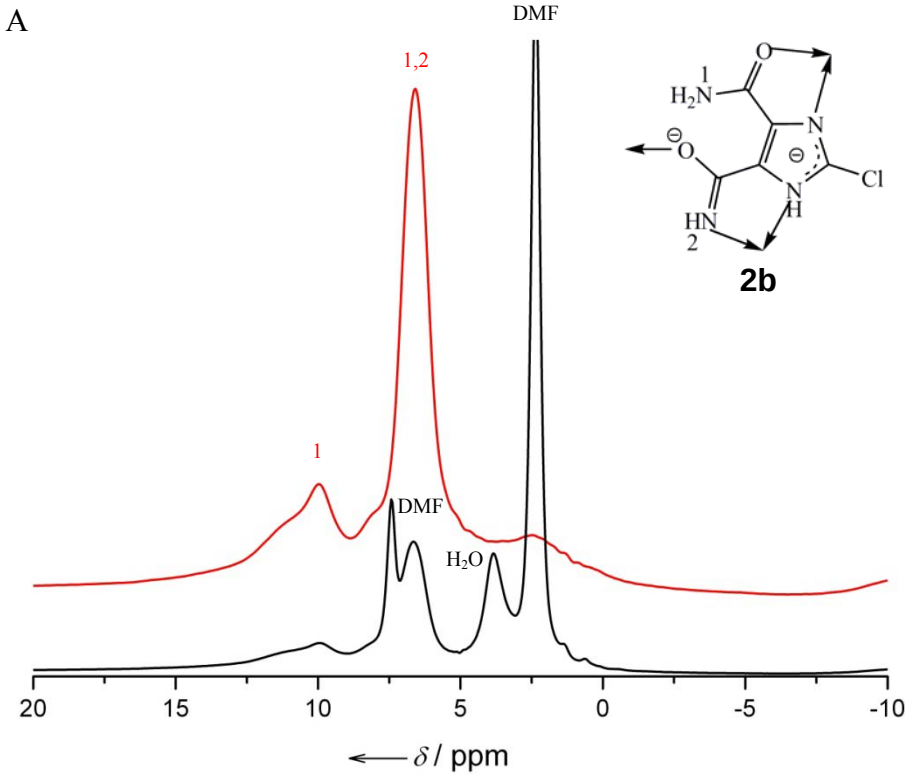

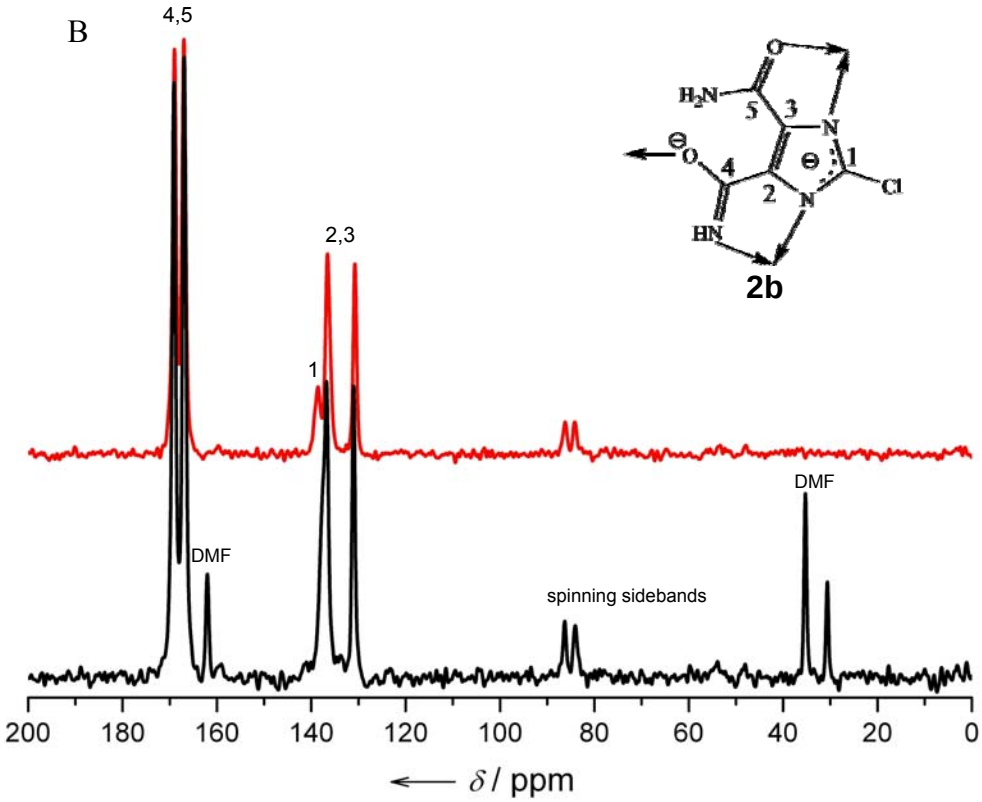

Figure S2-1 ^{1}H- (**A**) and ^{13}C- (**B**) CPMAS NMR spectra of IFP-2 (black – as synthesized, red – activated), activation procedure: 200°C and 10^{-3} mbar, 3 days.

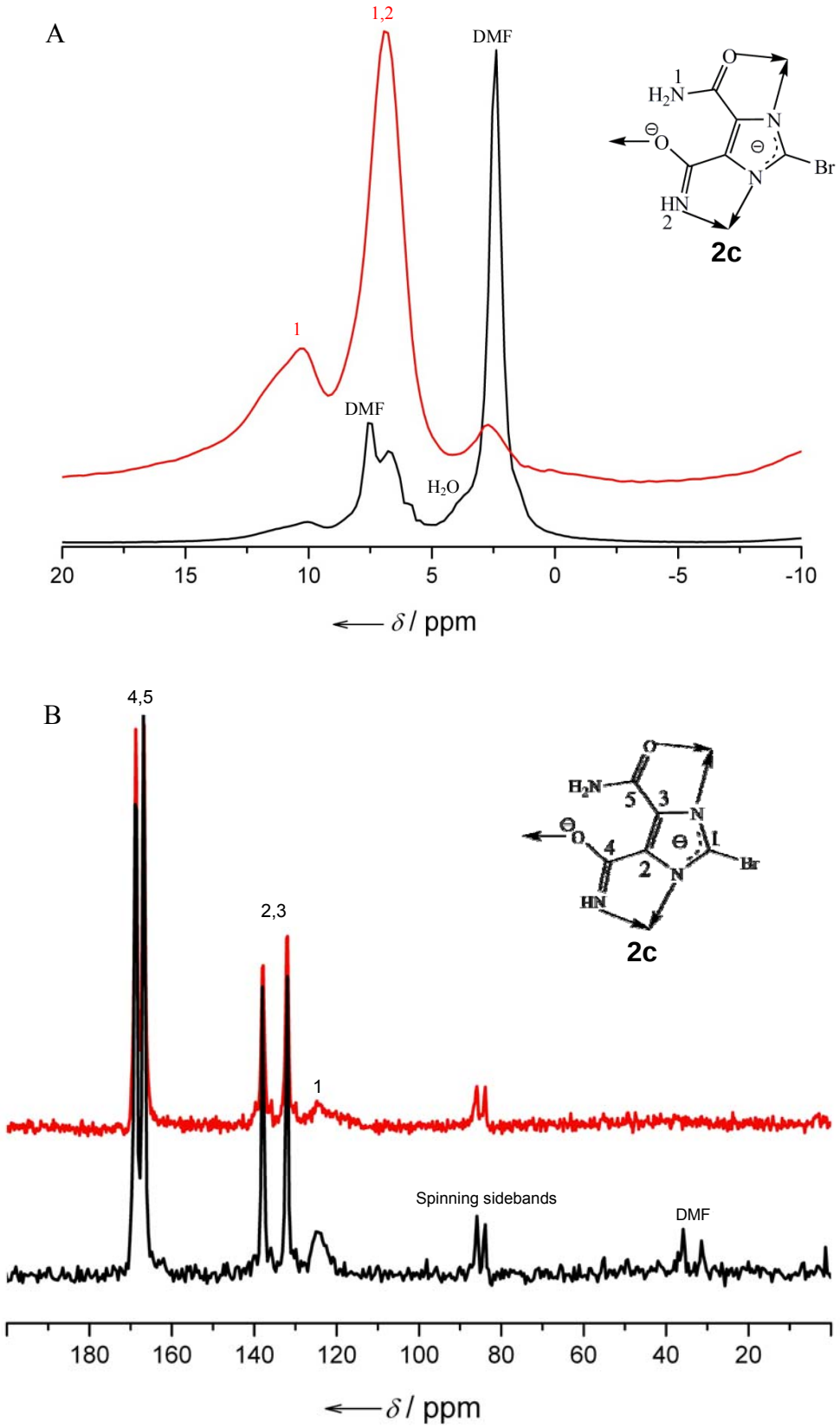

Figure S2-2 ^{1}H- (**A**) and ^{13}C- (**B**) CPMAS NMR spectra of IFP-3 (black – as synthesized, red – activated), activation procedure: 200°C and 10^{-3} mbar, 3 days.

Powder X-ray-diffraction patterns

Powder X-ray diffraction (PXRD) patterns of all IFPs were measured on a Siemens Diffractometer D5005 in Bragg-Brentano reflection geometry. The diffractometer was equipped with a copper tube, a scintillation counter, automatical incident- and diffracted-beam soller slits and with a graphite secondary monochromator. The generator was set to 40 kV and 40 mA. All measurements were performed with sample rotating. Data were collected digitally from 3° to 70° 2θ using a step size of 0.02° 2θ and a count time of 4 seconds per step. The simulated powder pattern for IFP-2 and IFP-3 was calculated using single-crystal X-ray diffraction data and processed by the free Mercury v1.4.2 program provided by the Cambridge Crystallographic Data Centre. Other theoretical PXRD were calculated out of structure model of IFP-4 which have been constructed and optimized with the density functional *ab initio* calculations.

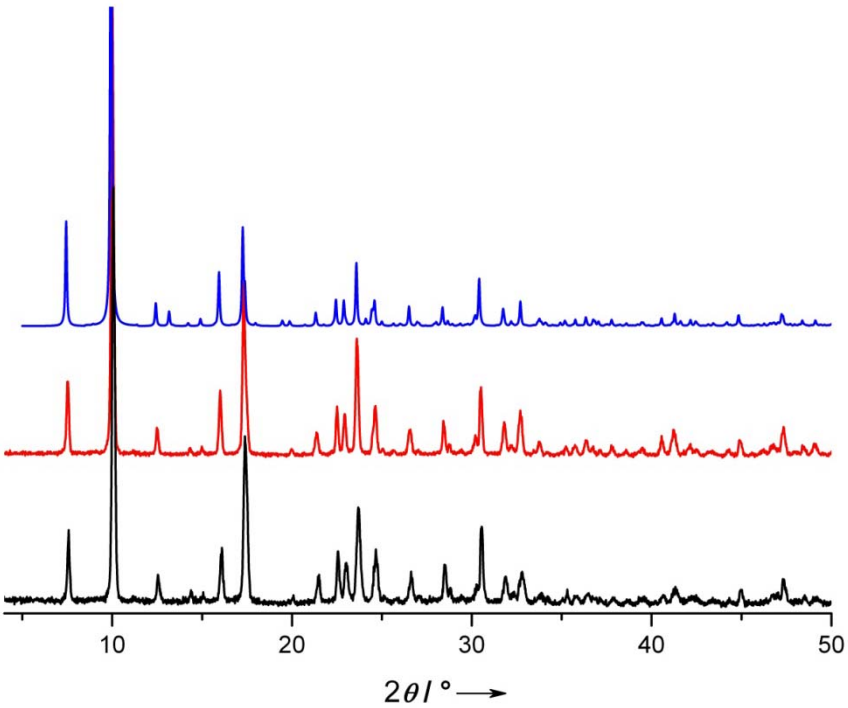

Figure S3-1 Powder X-ray diffraction patterns of IFP-2 (blue = simulated, red = as synthesized, black = activated).

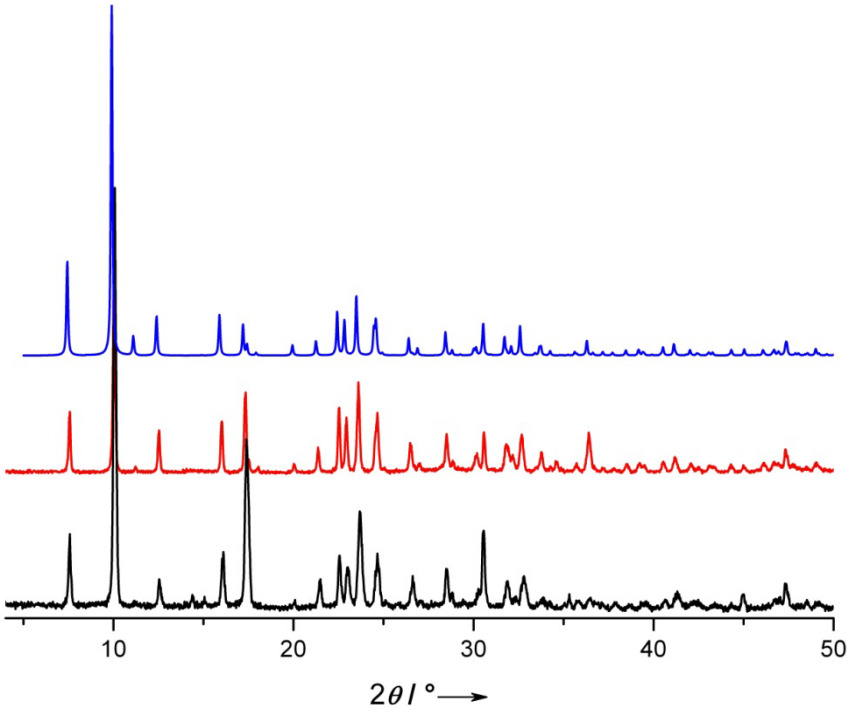

Figure S3-2 Powder X-ray diffraction patterns of IFP-3 (red = simulated, black = experimental).

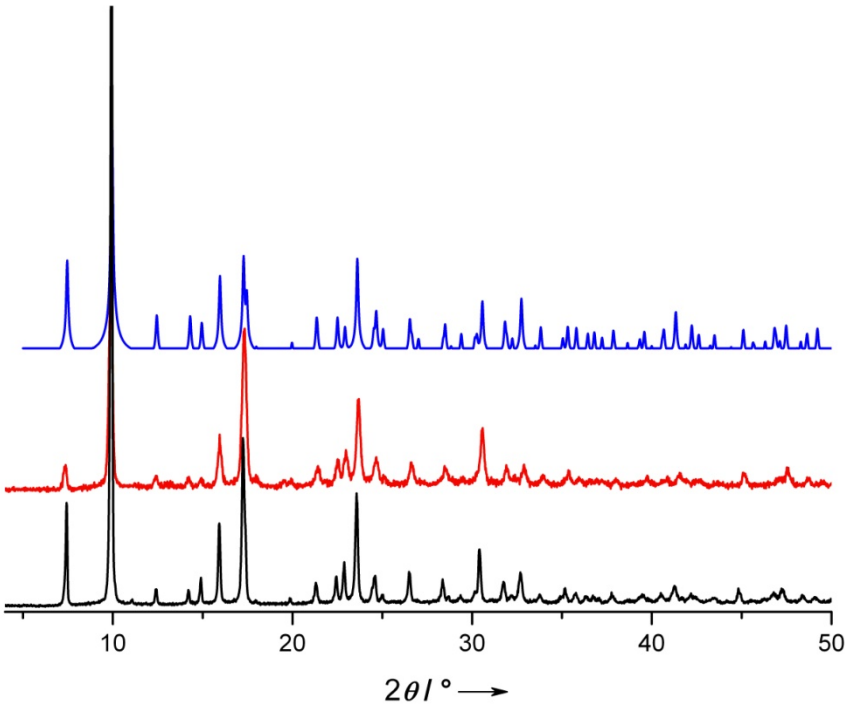

Figure S3-3 Powder X-ray diffraction patterns of IFP-4 (blue = simulated, red = as synthesized, black = activated).

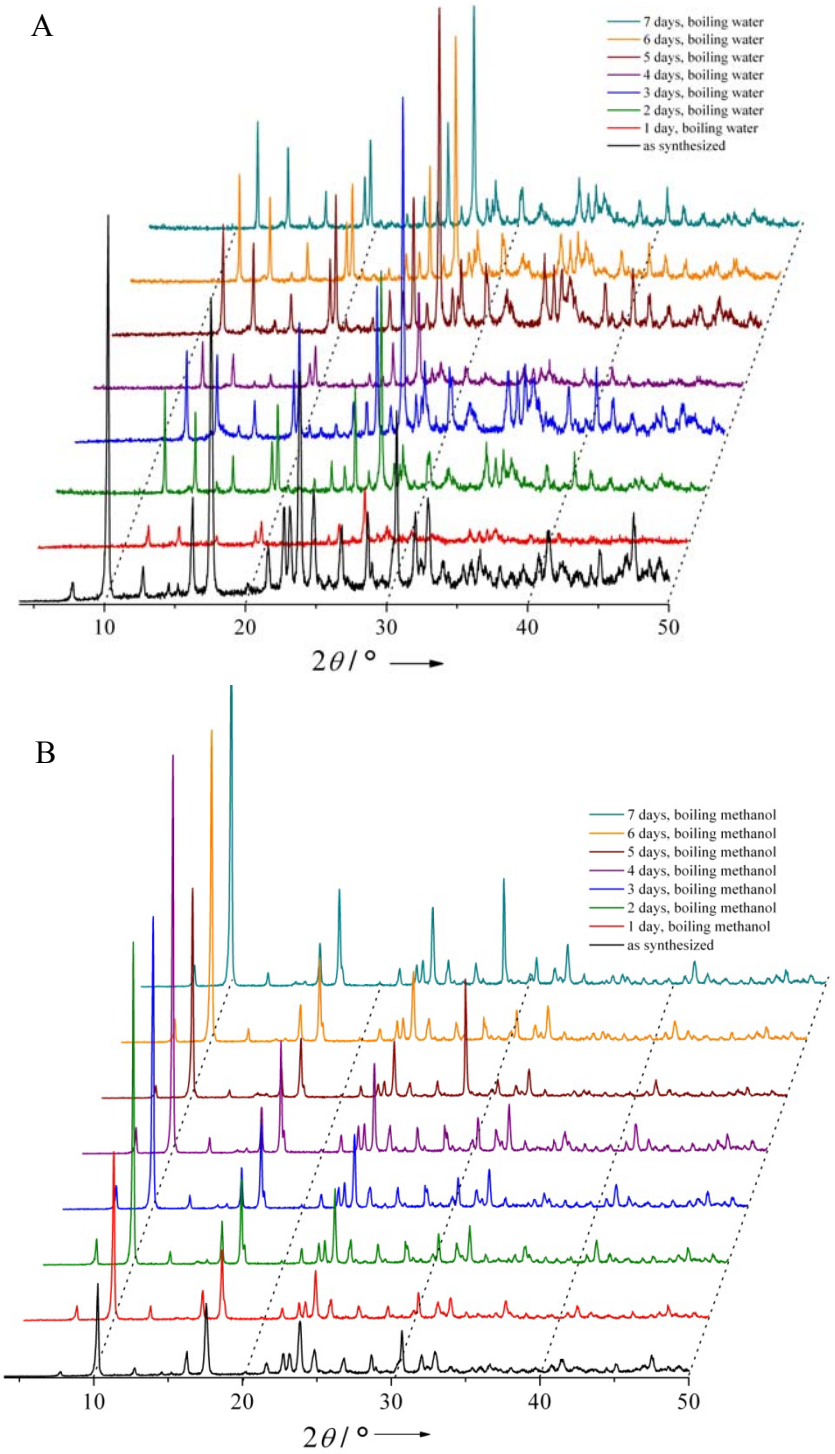
A
7 days, boiling water
6 days, boiling water
5 days, boiling water
4 days, boiling water
3 days, boiling water
2 days, boiling water
1 day, boiling water
as synthesized
10
20
30
40
50
2θ / °
B
7 days, boiling methanol
6 days, boiling methanol
5 days, boiling methanol
4 days, boiling methanol
3 days, boiling methanol
2 days, boiling methanol
1 day, boiling methanol
as synthesized
10
20
30
40
50
2θ / °

C

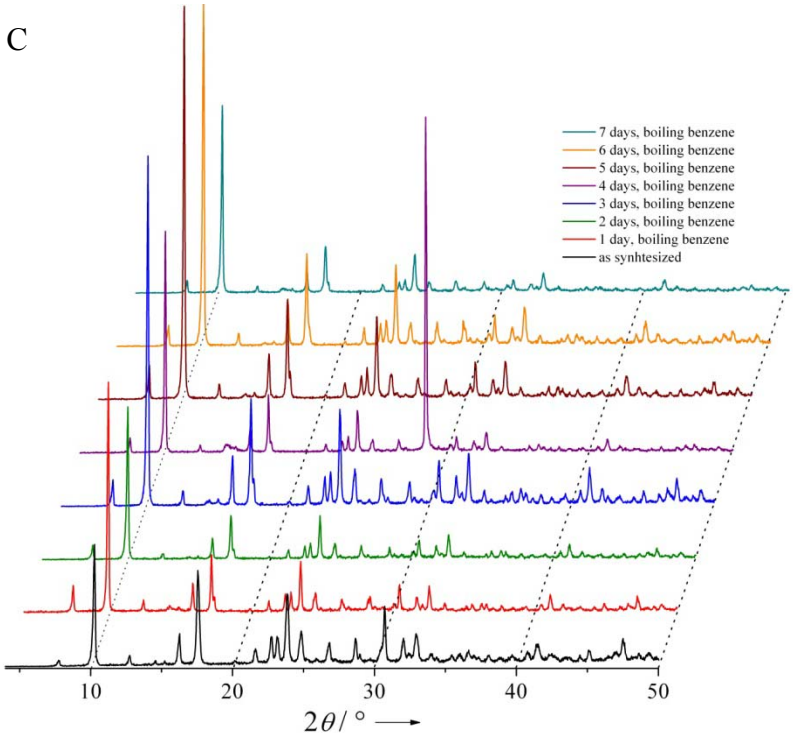

Figure S4-1 Powder X-ray diffraction patterns of IFP-2 collected during stability tests in refluxing water (A), methanol (B), and benzene (C).

A

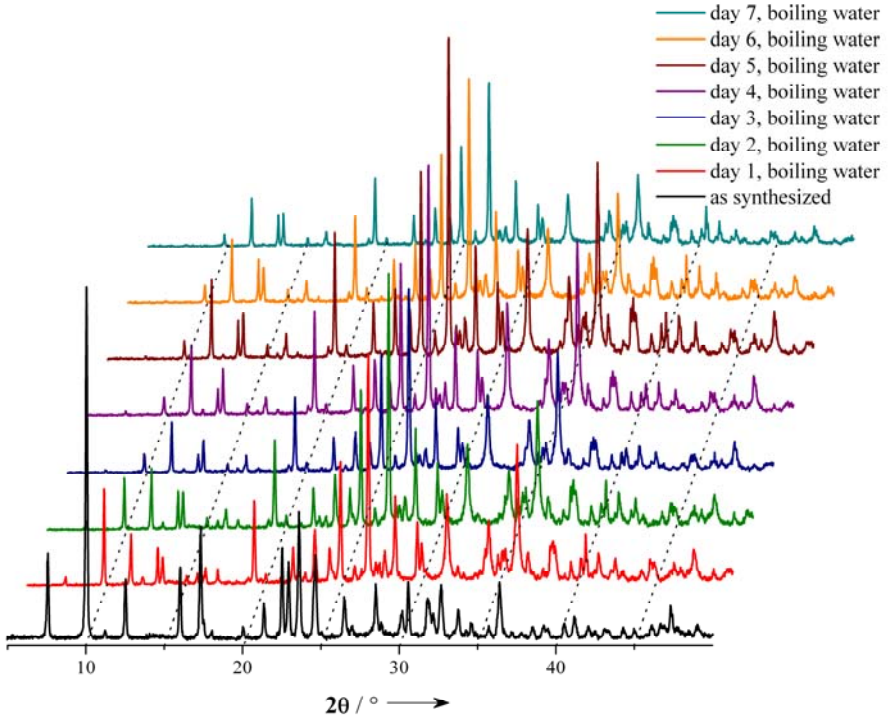

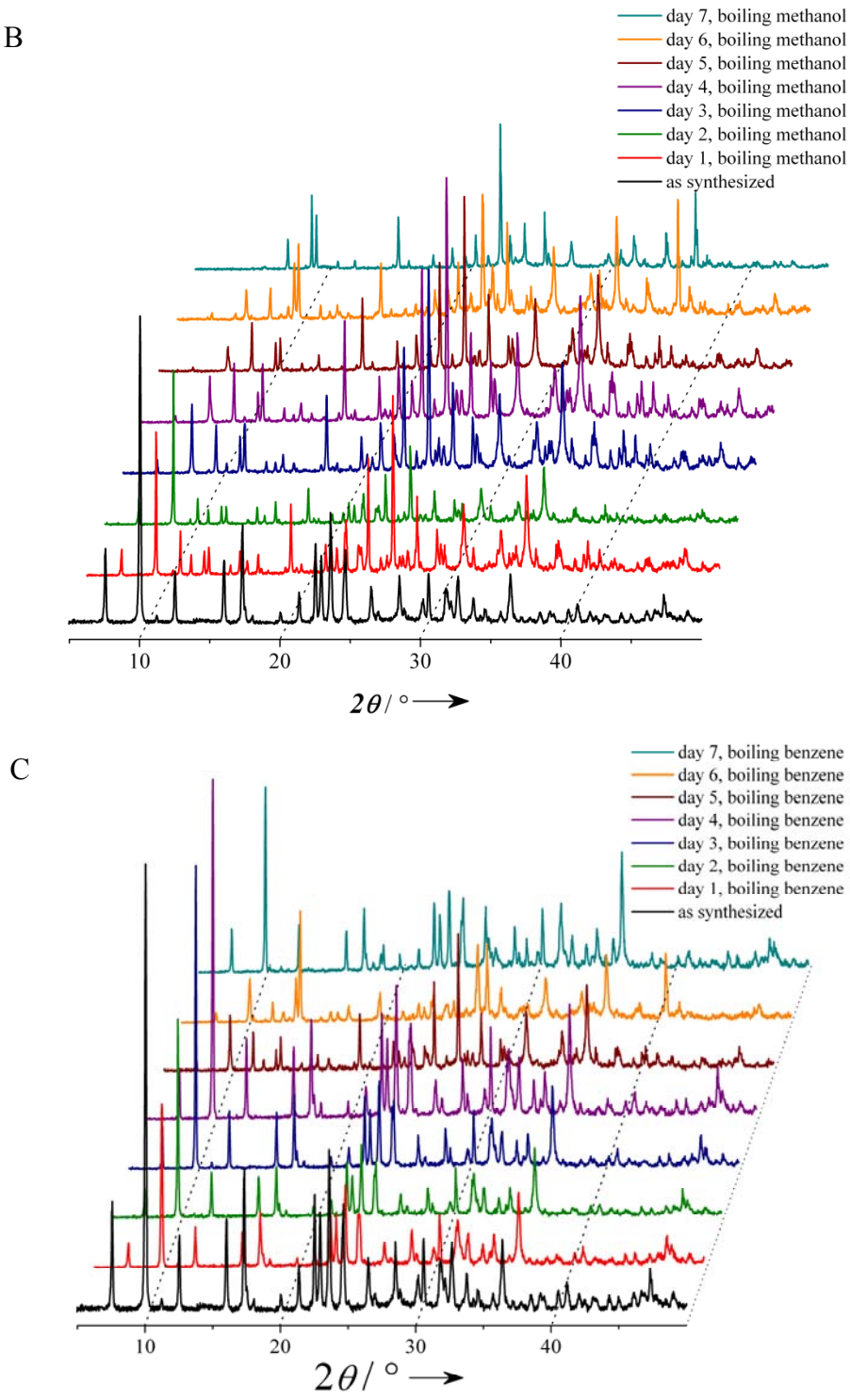

Figure S4-2 Powder X-ray diffraction patterns of IFP-3 collected during stability tests in refluxing water (A), methanol (B), and benzene (C).

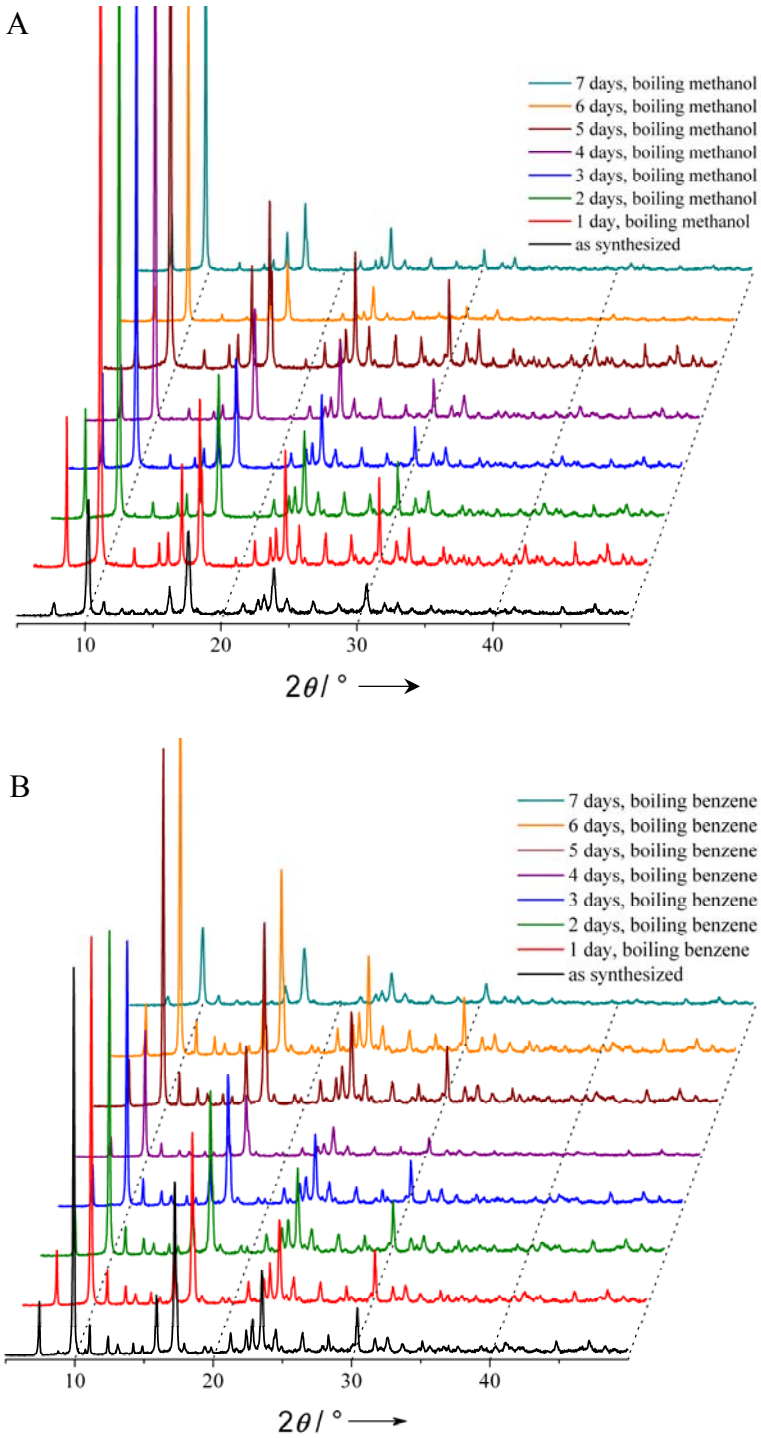

Figure S4-3 Powder X-ray diffraction patterns of IFP-4 collected during stability tests in refluxing methanol (A) and benzene (B).

Single crystal X-ray structure determinations:

The crystals were embedded in perfluoropolyalkylether oil and mounted on a glass fibre. Intensity data were collected at 210 K using a STOE Imaging Plate Diffraction System IPDS-2 with graphite monochromatized $Mo_{K\alpha}$ radiation (λ = 0.71073 Å) at 50 kV and 40 mA. The data were corrected by a spherical absorption correction using the program X-Area (Stoe, 2004) as well as for Lorentz, polarisation and extinction effects. The structure was solved with direct methods using SHELXS-97[4] and refined with full-matrix least-squares on F^2 using the program SHELXL-97[5]. All non-hydrogen atoms were refined anisotropically. The hydrogen atoms were located from the difference Fourier map and refined with $U_{iso}(H) = 1.2\ U_{eq}(N)$. In the case of IFP-3 the N—H(imine) distance was restrained to be 0.90 Å. The unit cell contains channels filled with disordered water molecules. In spite of several attempts, no reasonable solution could be received for the solvent (water) species in the channels of the crystal material. Very high displacement parameters, high esdimates and partial occupancy due to the disorder make it impossible to determine accurate atomic positions for the water molecules. PLATON/SQUEEZE[6] calculated the solvent-accessible void volume in the unit cell (IFP-2: 2111.0 $Å^3$ consistently with 41.0 % of the total cell volume; IFP-3: 2016.2 $Å^3$ consistently with 39.0 % of the total cell volume). These values correspond to the number of electrons, i.e. the residual electron density after the last refinement cycle, per cell (IFP-2: 405.0; IFP-3: 462.1). Those numbers of electrons agree with the roughly number of water molecules of 2.3 and 2.5, respectively (IFP-2: 2.25 x 10 x 18=405; IFP-3: 2.57 x 10 x 18=462). The contribution of the disordered solvent species was subtracted from the structure factor calculations. The deposited atom data (cif) reflect only known cell content.

Table S1. Crystal data, details of intensity measurements, and structure refinements for [Zn(2b)]· 2.3 H_2O (IFP-2) and [Zn(2c)]·2.5 H_2O (IFP-3).

	IFP-2	IFP-3
Empirical formula	$C_5H_{7.6}ClN_4O_{4.3}Zn$	$C_5H_8BrN_4O_{4.5}Zn$
Formula weight / g·mol^{-1}	293.37	341.43
Crystal system	trigonal	trigonal
Space group	*R*-3	*R*-3
cell dimensions		
$a = b$ / Å	17.8709(9)	17.8954(14)
c / Å	18.6382(10)	18.6250(16)
$\alpha = \beta$ / °	90	90
γ / °	120	120
Volume / Å^3	5155.0(5)	5165.5(7)
Temperature / K	210	210
Z	18	18
Density (calculated)/ g·cm^{-3}	1.674	1.715
Absorptions coefficient / cm^{-1}	2.380	5.597
2Θ range / °	3.42 – 49.96	3.42 – 49.96
crystal size / mm	0.12 x 0.11 x 0.09	0.17 x 0.14 x 0.09
F(000)	2563	3006
Index ranges	$-21 \le h \le 21$, $-21 \le k \le 21$, $-20 \le l \le 22$	$-21 \le h \le 19$, $-21 \le k \le 21$, $-22 \le l \le 22$
Reflections collected	11123	11169
Independent reflections	2013 (R_{int} = 0.0246)	2024 (R_{int} = 0.0556)
Max. and min. transmission	0.4770 and 0.5919	0.5421 and 0.5356
Data / restraints / parameters	2013 / 0 / 128	2024 / 1 / 128
R_1 / wR_2 [$F > 2\sigma(F)$]	0.0228 / 0.0598	0.0446 / 0.1278
R_1 / wR_2 (all data)	0.0265 / 0.0610	0.0609 / 0.1334
GooF on F^2	1.043	0.969
Largest diff. peak and hole / e·Å^{-3}	0.252 and -0.352	0.687 and -0.896

$w = 1/[[\sigma^2(F_o^2)+(0.0361P)^2] + 4.4188P]$ where $P=(F_o^2+2F_c^2)/3$ for IFP-2

$w = 1/[\sigma^2(F_o^2)+(0.0918P)^2]$ where $P=(F_o^2+2F_c^2)/3$ for IFP-3

Table S2 Selected bond lengths [Å] and angles [°] for [Zn(2b)] · 2.3 H_2O (IFP-2) and [Zn(2c)] · 2.5 H_2O (IFP-3)

	IFP-2	IFP-3		IFP-2	IFP-3
Zn1 - O1	2.123(2)	2.128(4)	N4 – C5	1.295(3)	1.283(7)
Zn1 - O2	1.982(2)	1.978(4)	C1 – Cl(Br)1	1.710(2)	1.823(6)
Zn1 - N1	2.151(2)	2.142(4)	O1 – C2	1.257(3)	1.267(7)
Zn1 - N2	2.085(2)	2.091(4)	C2 – C3	1.473(3)	1.485(7)
Zn1 - N4	1.984(2)	1.989(5)	C5 – O2^{II}	1.280(3)	1.274(7)
C3 – C4^{III}	1.382(3)	1.372(7)	C1 – N-1^{III}	1.331(3)	1.343(7)
C4 – C5	1.475(3)	1.495(8)	N1 – C4	1.371(3)	1.360(7)
N2 – C3	1.369(3)	1.365(8)	N2 - C1	1.319(3)	1.338(7)
N3 – C2	1.308(3)	1.292(9)			
O1 - Zn1 - O2	117.66(8)	118.1(2)	O1 - Zn1 - N1	85.89(6)	85.0(2)
O1 - Zn1 - N2	77.56(6)	77.1(2)	O1 - Zn1 - N4	121.30(8)	119.6(2)
O2 - Zn1 - N1	106.71(6)	107.2(2)	O2 - Zn1 - N2	89.09(6)	89.3(2)
O2 - Zn1 - N4	121.02(9)	122.2(2)	O1 – C2 - N3	122.9(2)	124.2(5)
N1 - Zn1 - N2	161.17(7)	160.0(2)	N1 - Zn1 - N4	79.32(7)	79.7(2)
N2 - Zn1 - N4	101.59(7)	101.5(2)	C4^{III} – C3 – C2	136.7(2)	137.5(6)

Symmetry operators: ^{I} 2/3-y,-2/3+x-y,1/3+z ^{II} 1/3+x-y,x-1/3,2/3-z ^{III} 4/3-x+y,2/3-x,z-1/3 ^{IV} 2/3+y,1/3-x+y,1/3-z ^{V} -1/3+x-z,x-2/3,1/3-z ^{VI} 1/3+y,2/3-x+y,2/3-z ^{VII} 4/3-x,-1/3-y,2/3-z

Table S3 Hydrogen-bonding parameters [Å, °] for [Zn(2b)] · 2.3 H_2O (IFP-2) and [Zn(2c)] · 2.5 H_2O (IFP-3)

	IFP-2				IFP-3			
N3 - H3A … O2^{IV}	0.81(4)	2.02(4)	2.798(3)	161(3)	1.03(9)	1.83(9)	2.802(6)	155(7)
N3 - H3B … O1^{VII}	0.91(4)	2.11(4)	3.021(3)	171(3)	0.72(9)	2.30(9)	3.018(6)	175(9)
N4 - H4 … N1^{II}	0.77(3)	2.49(3)	3.207(3)	157(3)	0.99(2)	2.40(4)	3.219(7)	154(6)

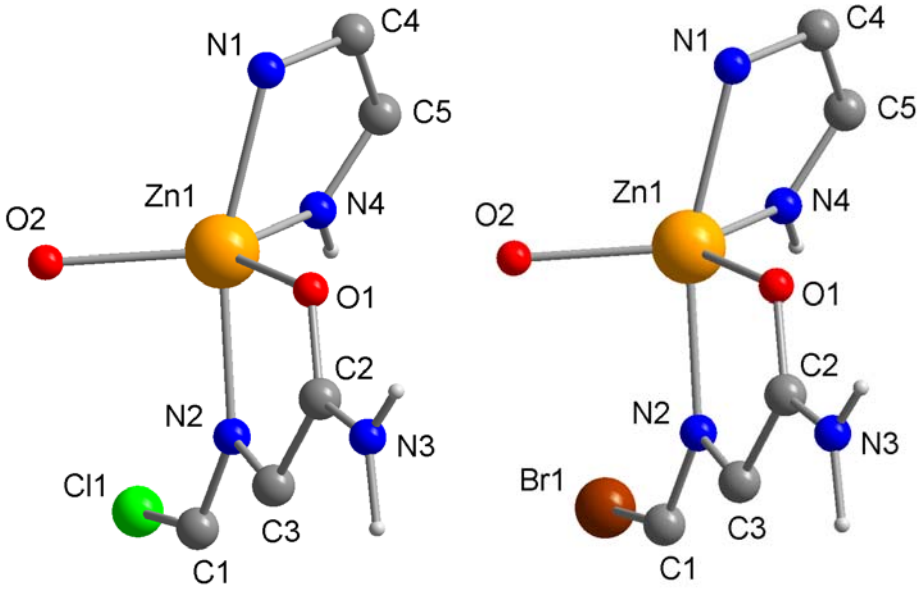

Figure S5-1 Asymmetric units of IFP-2 (left side) and IFP-3 (right side).

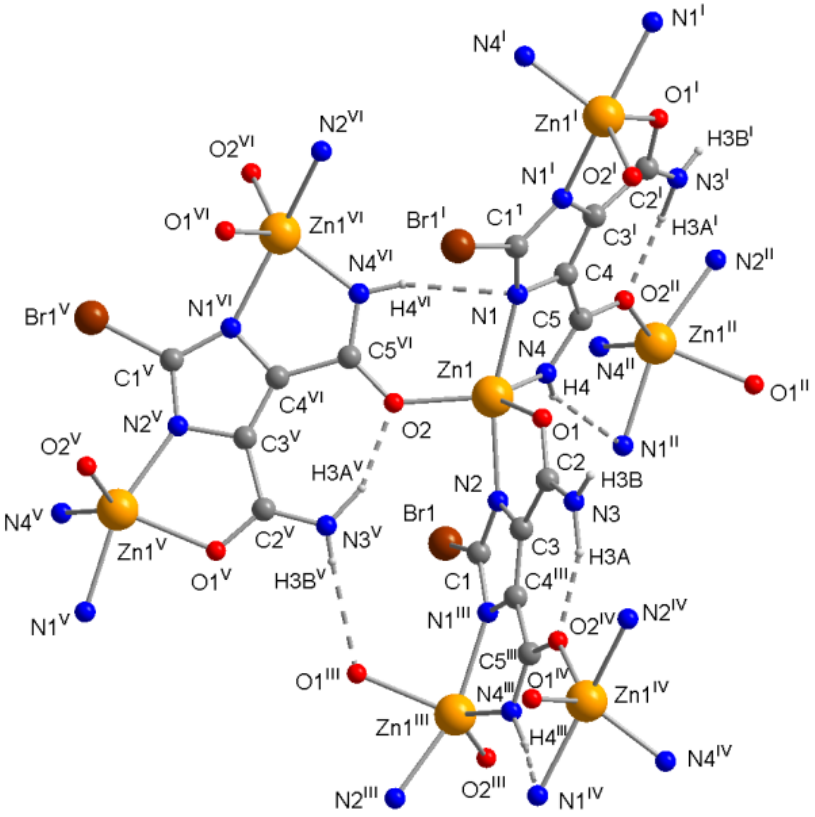

Figure S5-2 Crystal structure of IFP-3 showing the coordination environment of Zn^{II}, the coordination mode of linker 2c, and the hydrogen bonds (dotted lines). For the symmetry codes and for details of the hydrogen bonds, see Table S2 and S3.

Thermogravimetric (TG) analysis

The TG measurements were performed in a stationary air atmosphere (no purge) from room temperature up to 800 °C using a Linseis thermal analyzer (Linseis, Germany) working in the vertical mode. The heating rate was 10 °C/min. The samples were placed in cups of aluminium oxide.

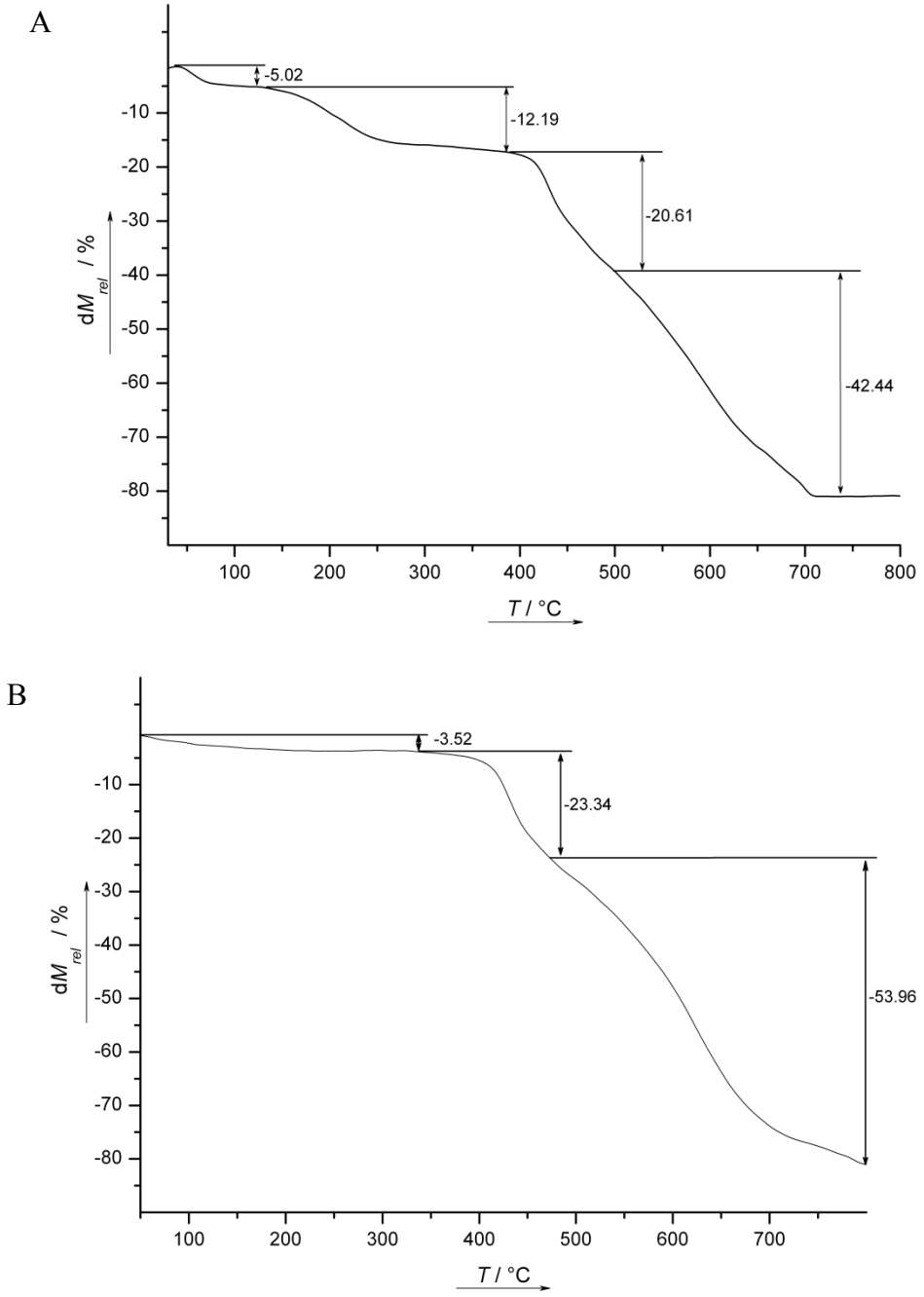

Figure S6-1 TGA measurements of **A)** as synthesized und **B**) activated compound IFP-2.

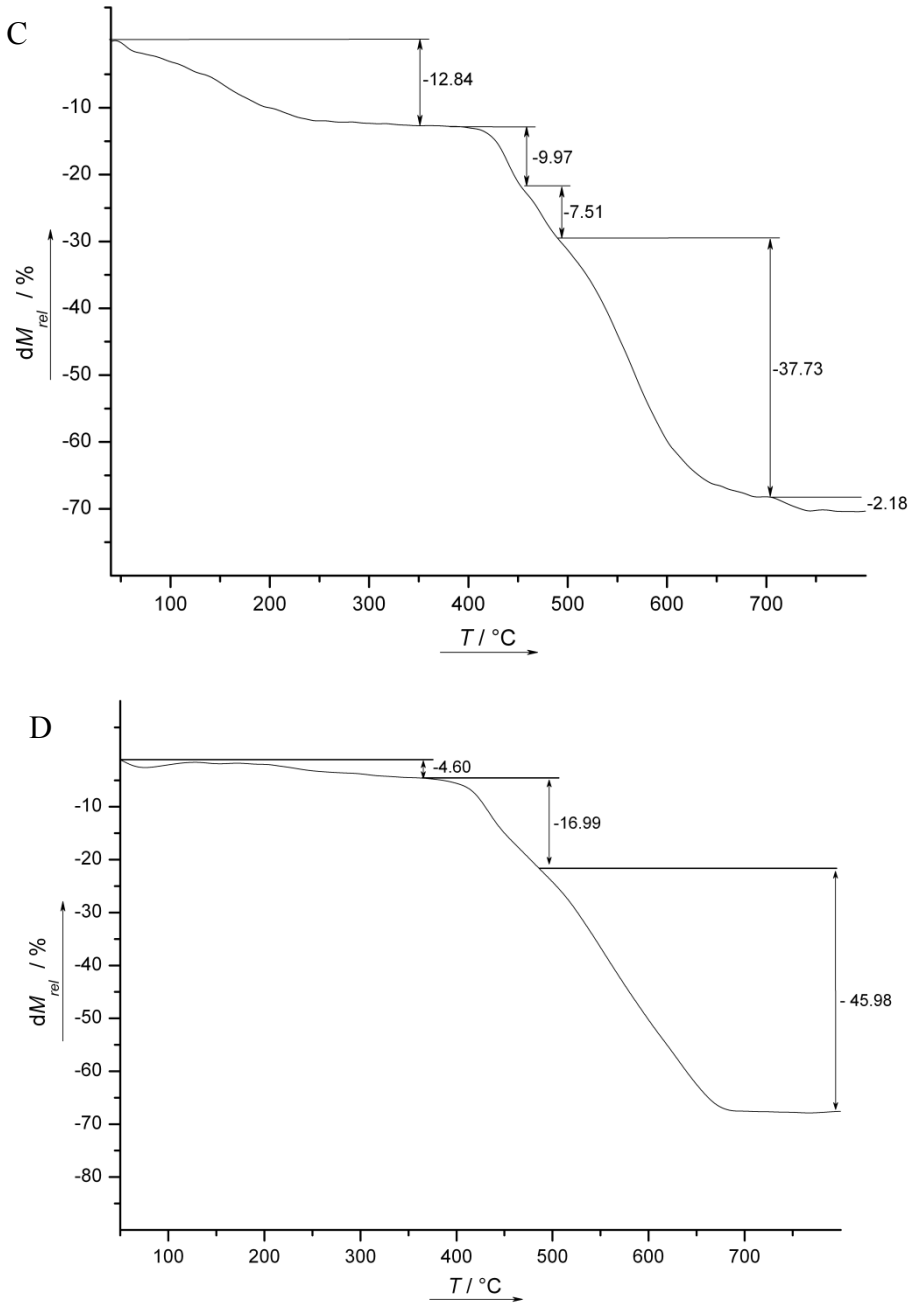

Figure S6-2 TGA measurements of **A)** as synthesized and **B**) activated compound IFP-3.

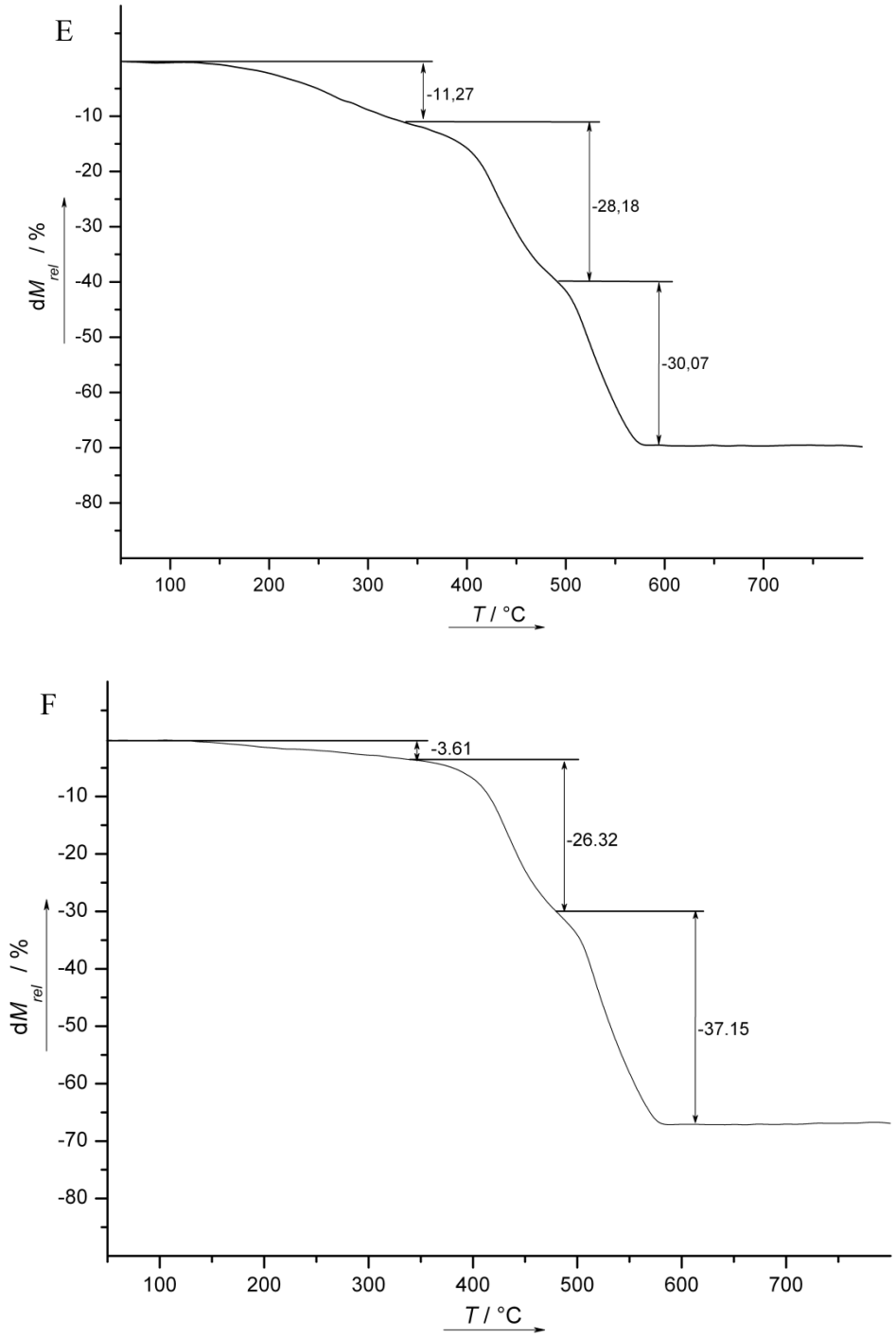

Figure S6-3 TGA measurements of IFP-4: **A)** as synthesized, **B**) activated compound.

Physisorption properties

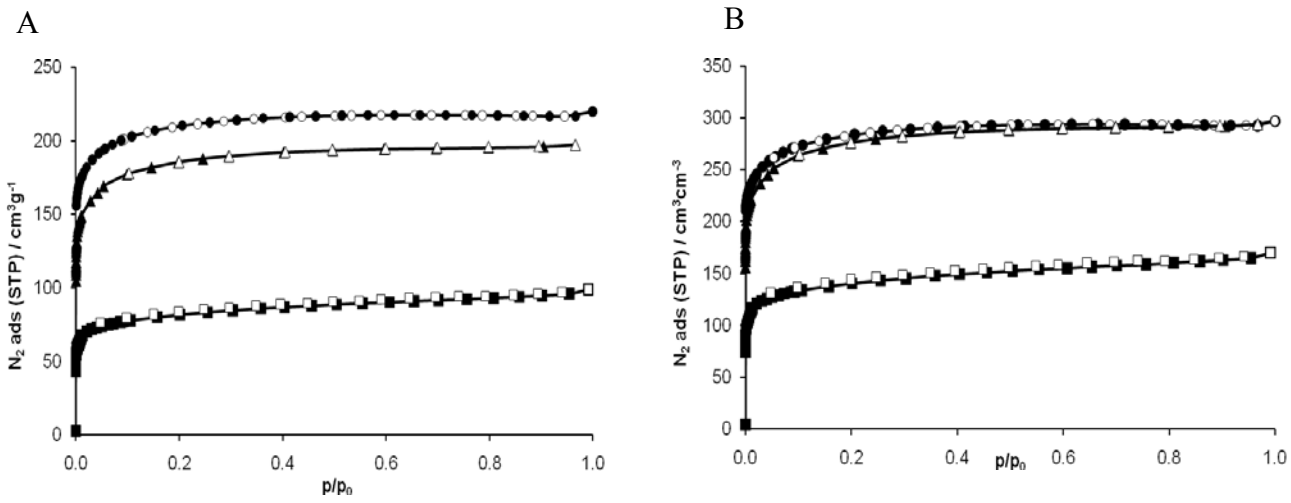

Figure S7 Experimental nitrogen adsorption (closed symbols)/desorption (open symbols) isotherms of IFP-1 (circles), IFP-2 (triangles) and IFP-3 (squares) at 77.3 K: **A** per g of activated MOF; **B** per cm^{-3} of activated MOF.

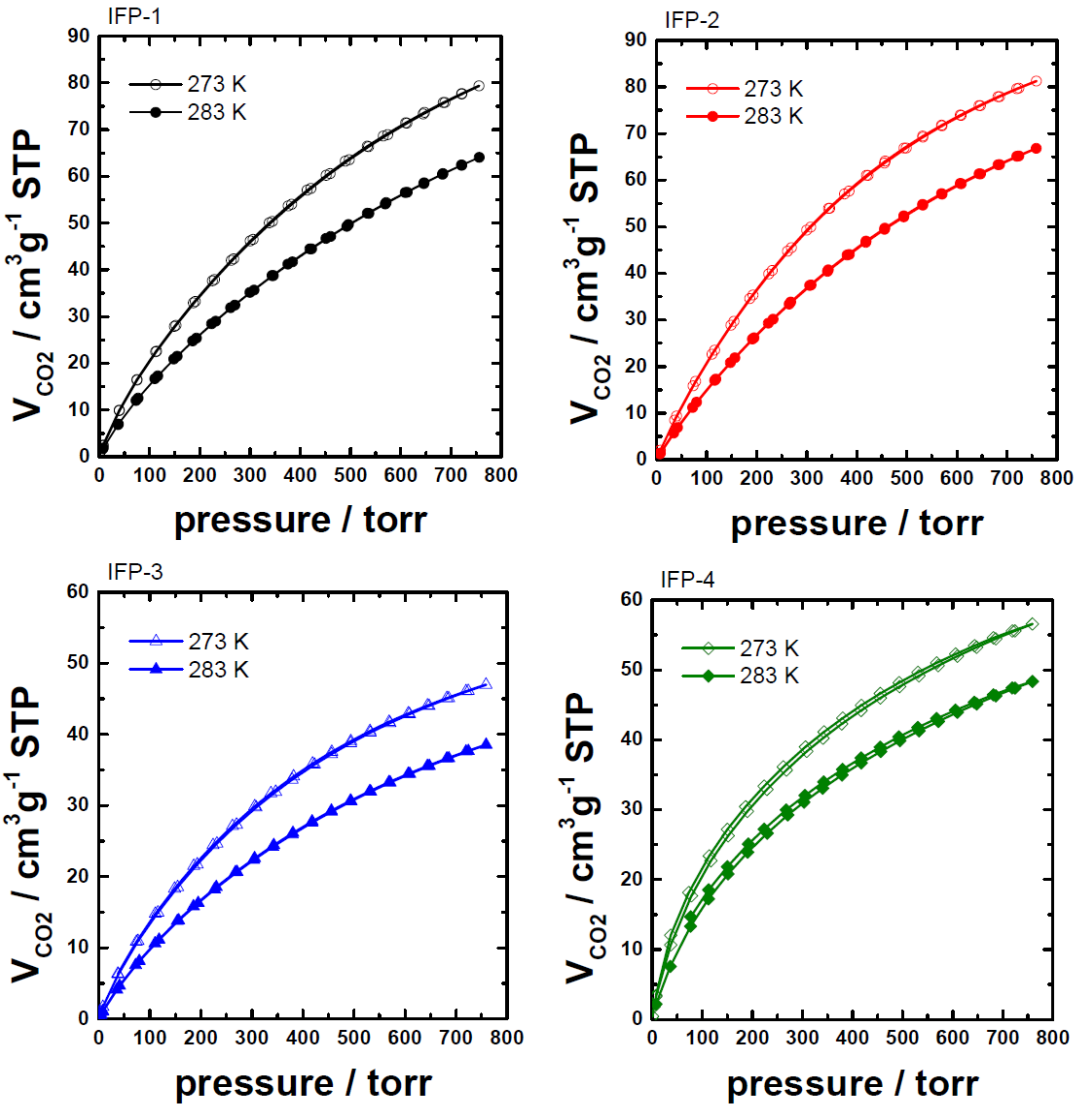

Figure S8-1 CO_2 adsorption/desorption isotherms measured at 273K and 283K for: IFP-1 (black); IFP-2 (red); IFP-3 (blue) and for IFP-4 (green).

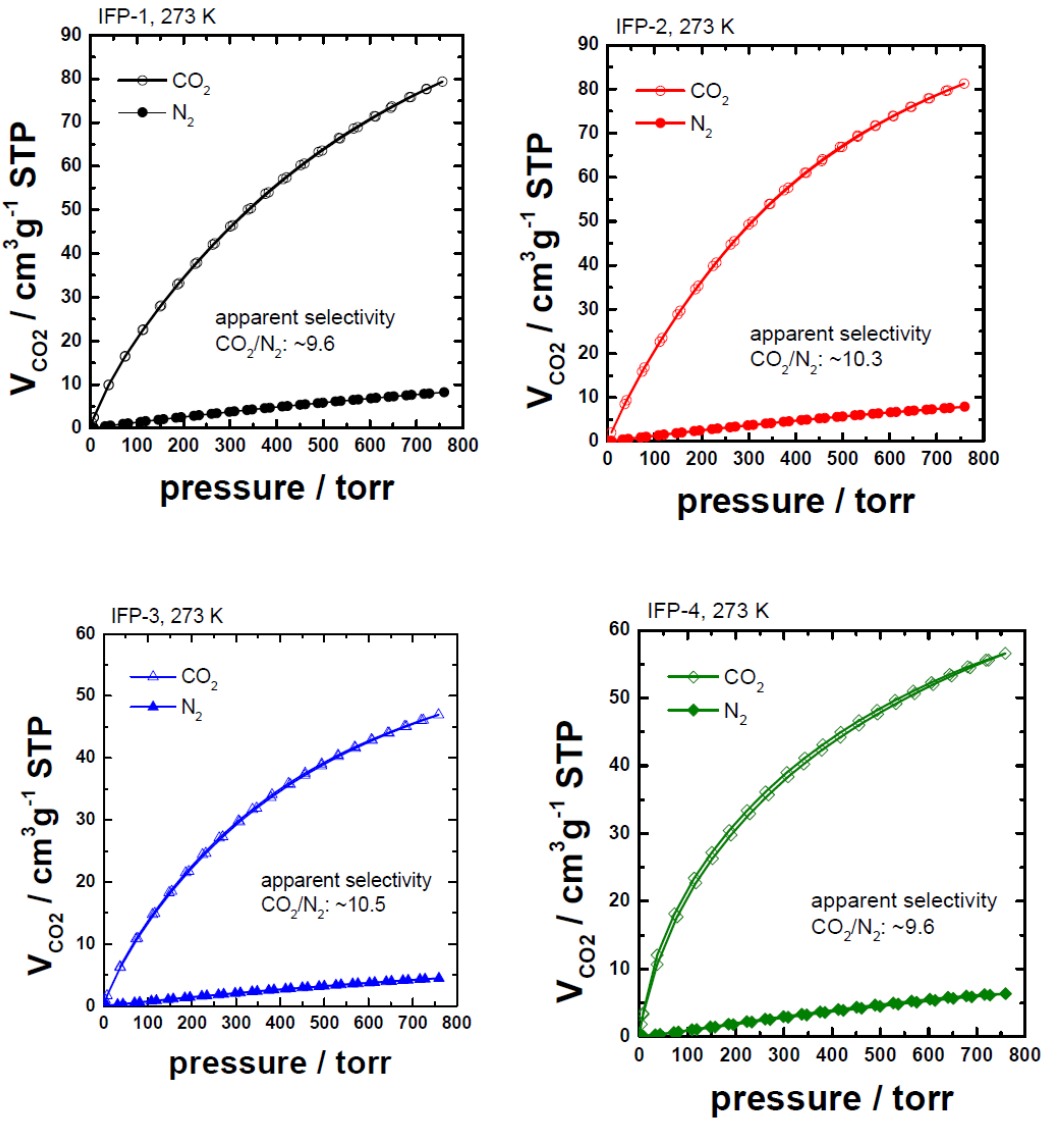

Figure S8-2 CO_2 and N_2 adsorption/desorption isotherms measured at 273K for: IFP-1 (black); IFP-2 (red); IFP-3 (blue) and for IFP-4 (green).

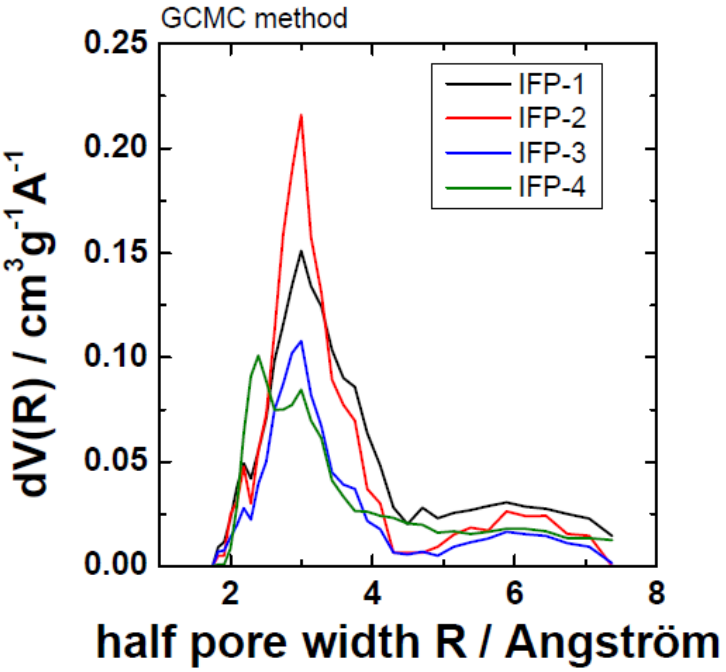

Figure S9-1. PSD obtained by GCMC analysis of the CO_2 adsorption isotherms measured at 273K.

The adsorption isotherms (CO_2, 273 K and 283 K) of IFP-1 and IFP-4 were fitted by a single Langmuir fit and by a dual-site Langmuir fit, which assumes the presence of two adsorption sites of different adsorption energy. Below are the plots, which show clearly, that the isotherms cannot be fitted by a single-site model, but by a dual site model. We furthermore analyzed the adsorption energies of the two sites (see Table below) and the maximum loadings.

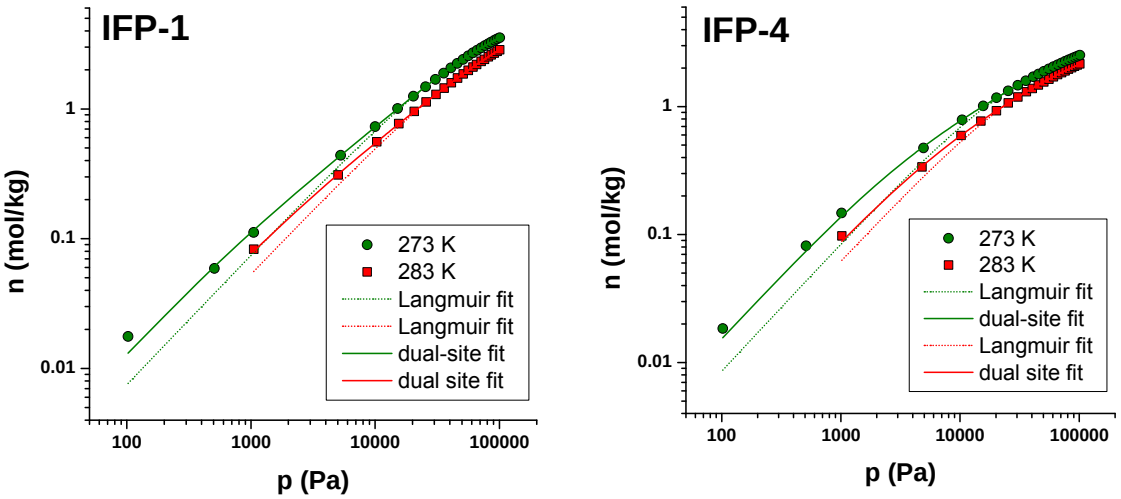

Figure S9-2. Plots of adsorption isotherms (CO_2, 273 K and 283 K) of IFP-1 and IFP-4 fitted by a dual-site Langmuir fit.

Table S4. Analysis of adsorption energies.

Langmuir fit: $n = \frac{q_{\max} K p}{1 + K p}$	*Dual-site fit (adsorption sites a and b of different capacity q_{max} and energy E):* $n = \frac{q_{\max,a} K_a p}{1 + K_a p} + \frac{q_{\max,b} K_b p}{1 + K_b p}$ *(with: $K = K_0 exp(E/RT)$)*

Dual site fit parameters:

IFP-1

$q_{max,a}$ (273 K) = 7.04 mol/kg

K_a (273 K) = 9.22278E-6

$q_{max,b}$ (273 K) = 0.162 mol/kg

(~3% of overall capacity)

K_b (273 K) = 4.09291E-4

$q_{max,a}$ (283 K) = 6.9 mol/kg

K_a (283 K) = 6.18039E-6

$q_{max,b}$ (283 K) = 0.222 mol/kg

K_b (283 K) = 1.7855E-4

E_a = 25.7 kJ/mol

E_b = 53.3 kJ/mol

IFP-4

$q_{max,a}$ (273 K) = 3.54 mol/kg

K_a (273 K) = 1.23999E-5

$q_{max,b}$ (273 K) = 0.58 mol/kg

(~14% of overall capacity)

K_b (273 K) = 1.93501E-4

$q_{max,a}$ (283 K) = 3.37 mol/kg

K_a (283 K) = 8.67634E-6

$q_{max,b}$ (283 K) = 0.64 mol/kg

K_b (283 K) = 1.00519E-4

E_a = 22.9 kJ/mol

E_b = 42 kJ/mol

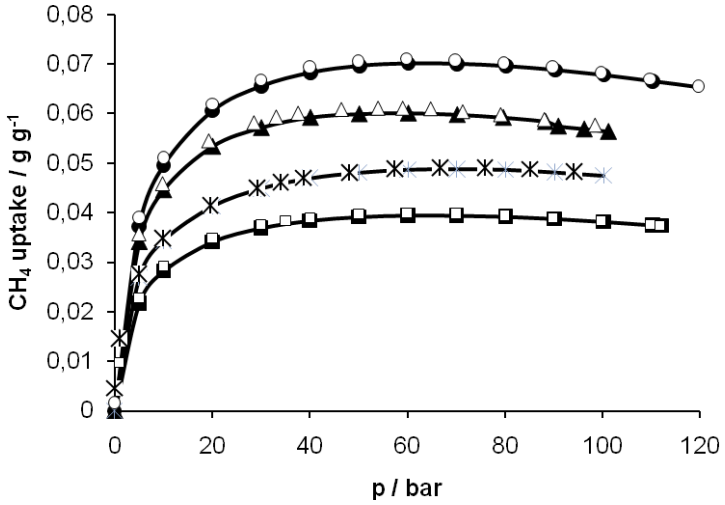

Figure S10. Experimental methane adsorption (closed symbols) and desorption (open symbols) isotherms of IFP-1 (circles), IFP-2 (triangles), IFP-3 (squares) and IFP-4 (stars) at 298 K

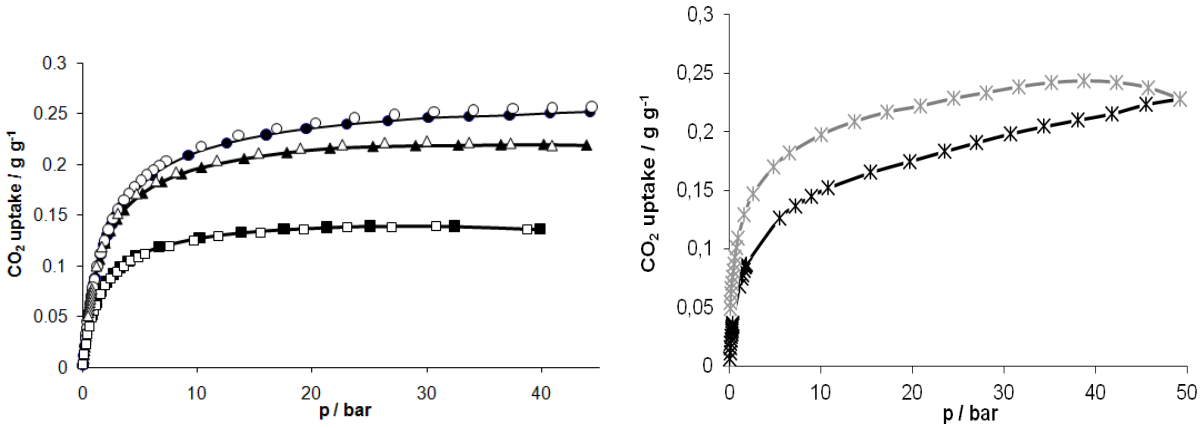

Figure S11. Left: Experimental carbon dioxide adsorption (closed symbols) and desorption (open symbols) isotherms of IFP-1 (circles), IFP-2 (triangles) and IFP-3 (squares) at 298K. Right: Experimental carbon dioxide adsorption (black symbols) and desorption (grey symbols) isotherms of IFP-4 (stars) at 298K.

Additional Theoretical section

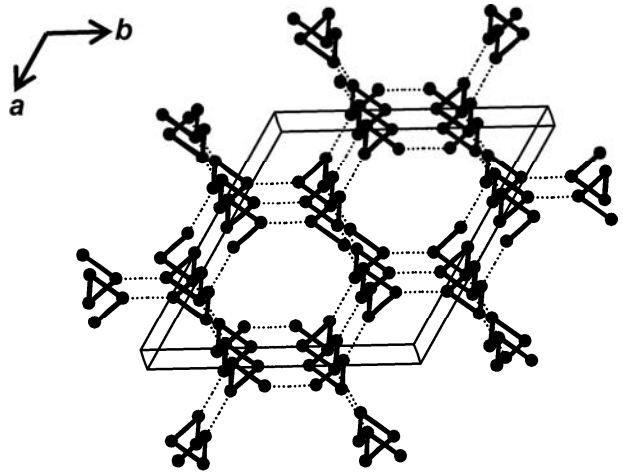

Figure S12 The underlying *helical* **etb** topology of IFPs: chains along [001] are linked (by dotted lines) to form a 3-connected net.

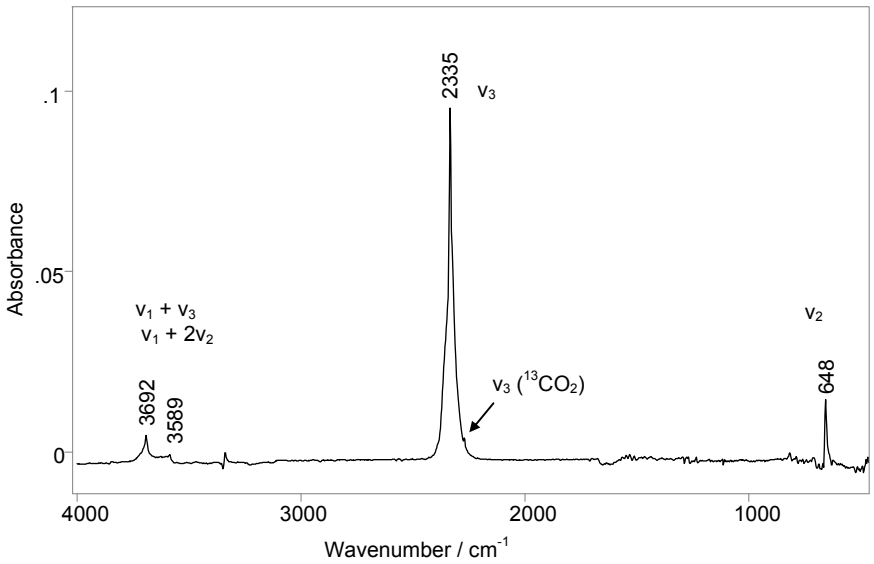

Figure S13. A typical IR spectrum of CO_2 adsorbed on IFPs. IFP-1 is presented here at a CO_2 pressure of 67 mbar. The noise on the spectrum is mainly attributed to the shifts in the bands when a small amount (<1mbar) CO_2 introduced into the cell.

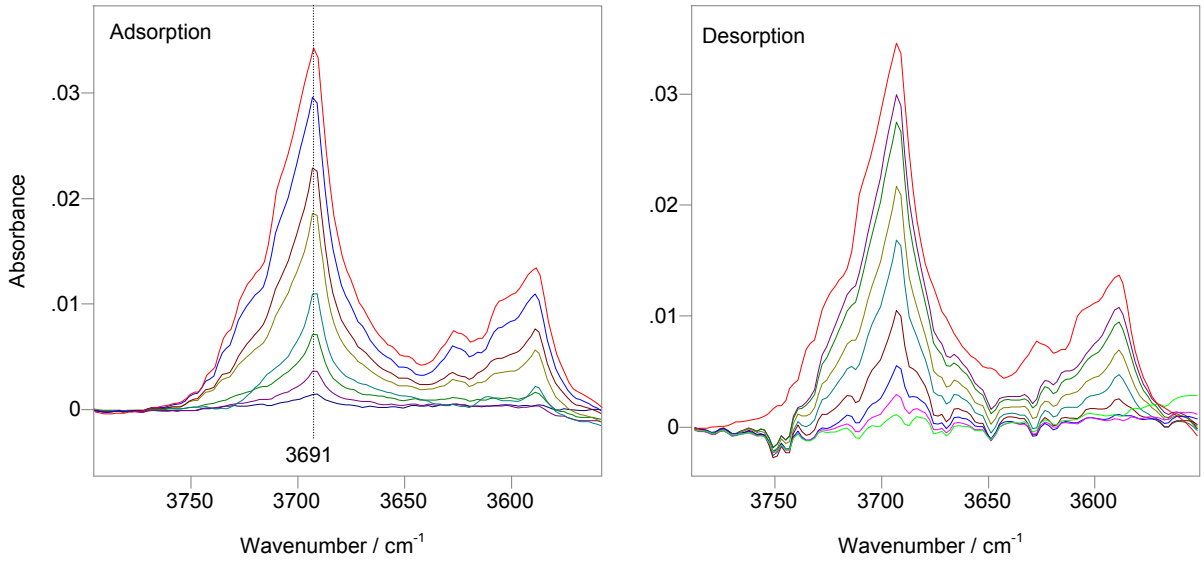

Figure S14. IR spectra of CO_2 adsorbed on IFP-1 in the adsorption and desorption ranges at different CO_2 pressures between 13 mbar and 1 bar. No shift in the combination bands have been observed with increasing pressures. According to the spectra in the desorption branch the CO_2 adsorption was fully reversible.

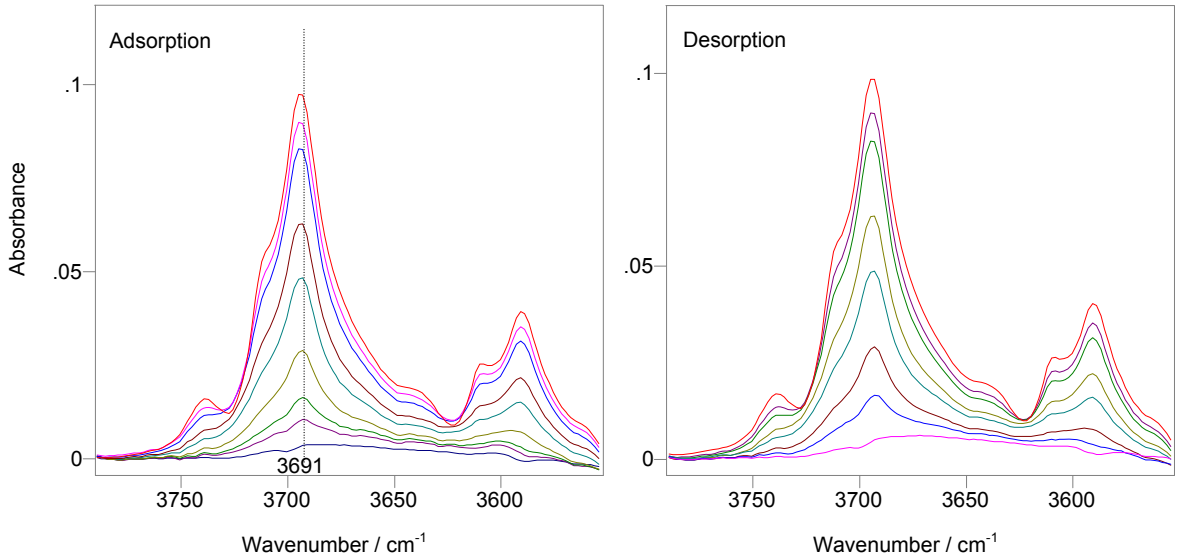

Figure S15. IR spectra of CO_2 adsorbed on IFP-2 in the adsorption and desorption ranges at different CO_2 pressures between 13 mbar and 1 bar. A shift to higher wavenumbers (2 cm^{-1} blue shift of the band at 3691 cm^{-1}) in the combination bands have been observed with increasing pressures. According to the spectra in the desorption branch the CO_2 adsorption was fully reversible.

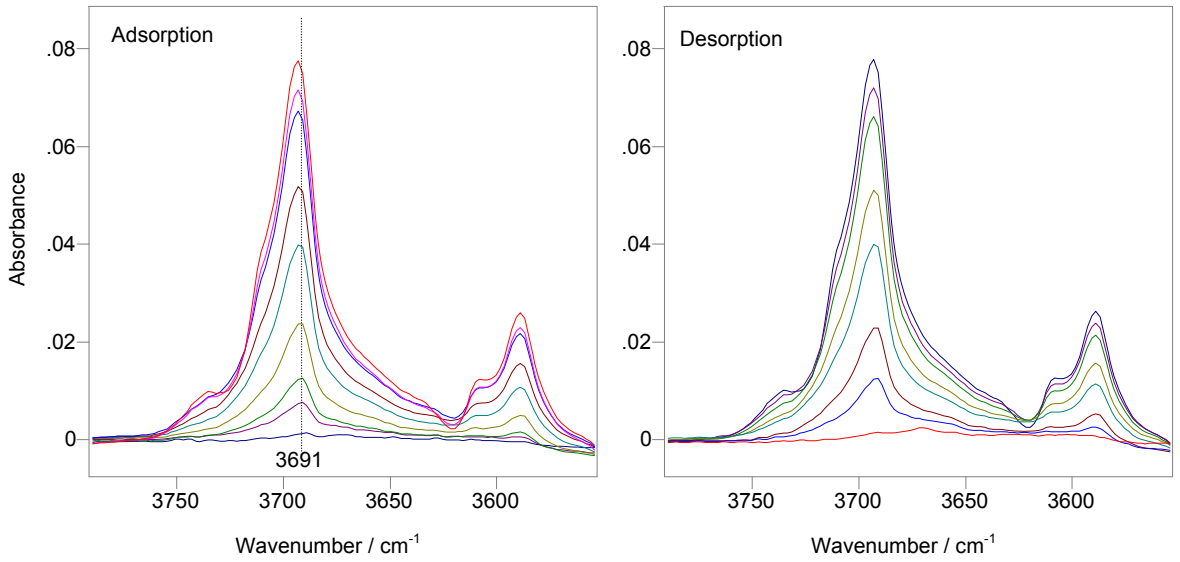

Figure S16. IR spectra of CO_2 adsorbed on IFP-3 in the adsorption and desorption ranges at different CO_2 pressures between 13 mbar and 1 bar. A shift to higher wavenumbers (2 cm^{-1} blue shift of the band at 3691 cm^{-1}) in the combination bands have been observed with increasing pressures. According to the spectra in the desorption branch the CO_2 adsorption was fully reversible.

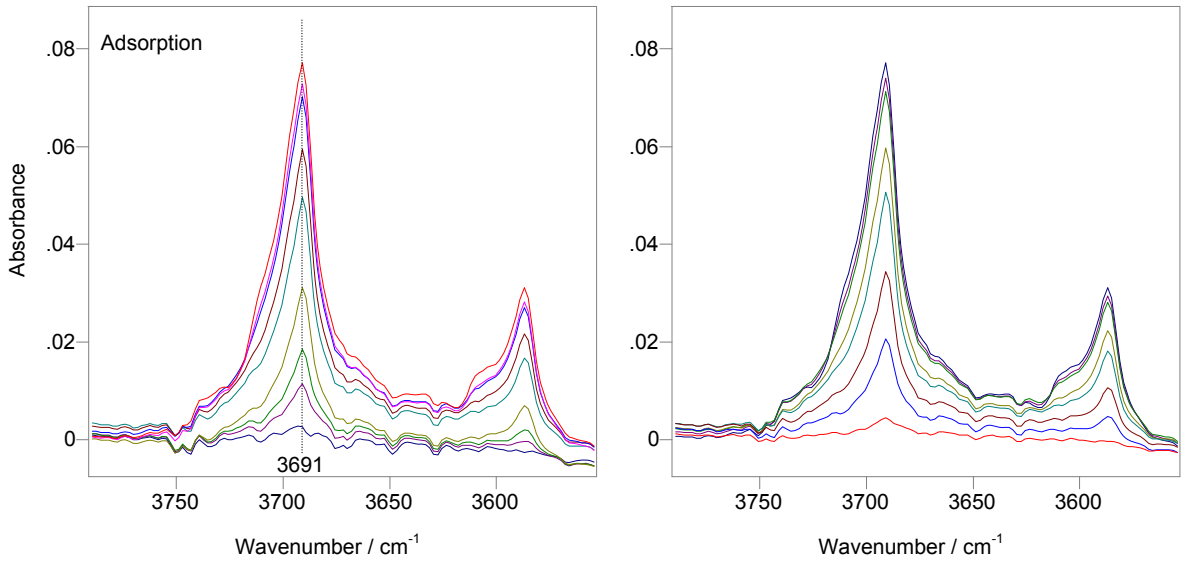

Figure S17. IR spectra of CO_2 adsorbed on IFP-4 in the adsorption and desorption ranges at different CO_2 pressures between 13 mbar and 1 bar. No shift in the combination bands have been observed with increasing pressures. According to the spectra in the desorption branch the CO_2 adsorption was fully reversible. (The compensation of the atmospheric water vapor is not perfect, note the ´noise level´).

Under practical conditions all gases contain some moisture. The stability of the adsorbents to water vapour and CO_2 capacity in the presence of water is an important issue. We therefore investigated the CO_2 adsorption if water vapour present in the CO_2 gas. The water is physisorbed on the IFP-1 as the broad OH stretching band of water appear on the IR spectra (Figure S18). The adsorption of the water does not effect very significantly the quantity of the adsorbed CO_2, however a 3% decrease can be observed determined from the IR spectra of IFP-1 contacted with 50 Torr CO_2 during the desorption. It is possible that the equilibrium time is longer for water adsorption. Comparing with the results of volumetric uptake of dry and wet CO_2 on IFP-1 (Figure S19), it seems that the increased uptake of wet CO_2 may correspond to the physisorption of the water vapour. Changes in the framework bands have not been observed on adsorption and desorption of water vapour.

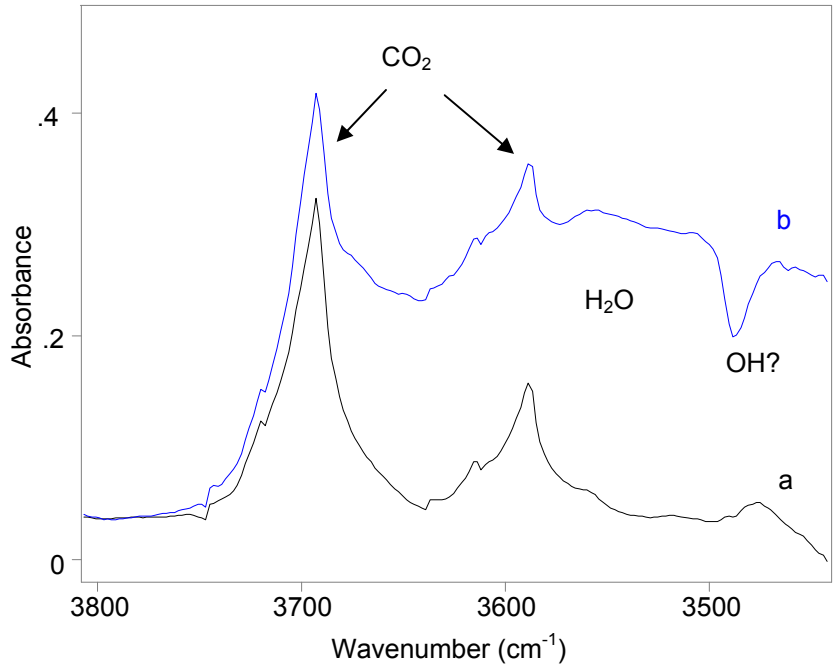

Figure S18. A region of the IR spectra of a) pure CO_2, and b) CO_2 with 2.1% water vapour adsorbed on IFP-1. CO_2 pressure 0.4 bar.

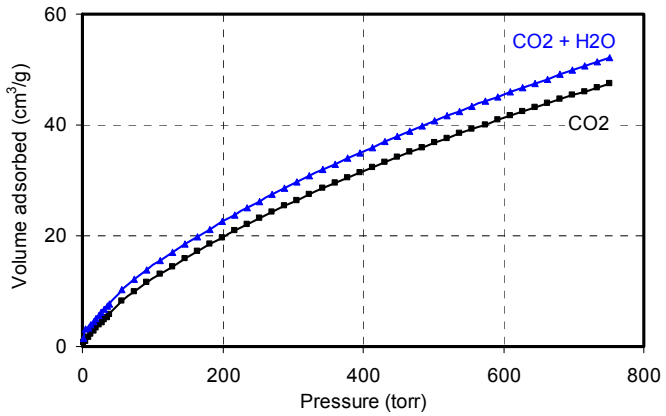

Figure S19. Dry and wet CO_2 uptake (volumetric adsorption measurements) of IFP-1 at the temperature of 25 °C

References

[1] E. C. Coad, J. Kampf, P. G. Rasmussen, *J. Org. Chem.* **1996,** 61, 6666-6672.

[2] P. G. Apen, P. G. Rasmussen, *Heterocycles* **1989**, 29, 1325-1329.

[3] H. Yanagisawa, Y. Amemiya, T. Kanazaki, Y. Shimoji, K. Fujimoto, Y. Kitahara, T. Sada, M. Mizuno, M. Ikeda, S. Miyamoto, Y. Furukawa, H. Koike, *J. Med. Chem.* **1996**, *39*, 323-338.

[4] G. M. Sheldrick, *SHELXS-97 Program for the Crystal Structure Solution*, University of Göttingen, Germany, **1997.**

[5] G. M. Sheldrick, *SHELXL-97 Program for the Crystal Solution Refinement*, University of Göttingen, Göttingen, **1997.**

[6] A. L. Spek, *PLATON*, Multipurpose Crystallographic Tool, Utrecht University, Utrecht, The Netherlands, **2008**.